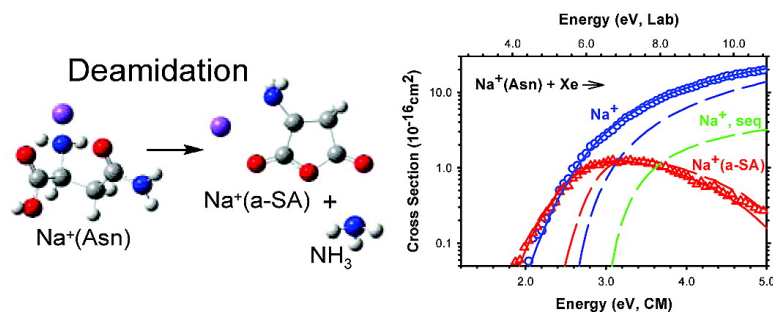


Thermodynamics and Mechanism of the Deamidation of Sodium-Bound Asparagine

A. L. Heaton, and P. B. Armentrout

J. Am. Chem. Soc., **2008**, 130 (31), 10227-10232 • DOI: 10.1021/ja801726g • Publication Date (Web): 10 July 2008

Downloaded from <http://pubs.acs.org> on February 8, 2009



More About This Article

Additional resources and features associated with this article are available within the HTML version:

- Supporting Information
- Links to the 2 articles that cite this article, as of the time of this article download
- Access to high resolution figures
- Links to articles and content related to this article
- Copyright permission to reproduce figures and/or text from this article

[View the Full Text HTML](#)

Thermodynamics and Mechanism of the Deamidation of Sodium-Bound Asparagine

A. L. Heaton and P. B. Armentrout*

Department of Chemistry, University of Utah, Salt Lake City, Utah 84112

Received March 7, 2008; E-mail: armentrout@chem.utah.edu

Abstract: The deamidation of asparagine (Asn) residues is the most common type of spontaneous post-translational protein modification and plays a vital role in inflammation, protein transformation, apoptosis, aging, and a number of degenerative diseases. Here we present a full molecular description of asparagine deamidation in the $\text{Na}^+(\text{Asn})$ complex by studying its collision-induced dissociation (CID) with Xe using a guided ion beam tandem mass spectrometer (GIBMS). Advanced methods for analysis of the energy-dependent CID cross section, considering both competing and sequential processes, provide the 0 K barrier for deamidation after accounting for unimolecular decay rates, internal energy of reactant ions, and multiple ion-neutral collisions. Relaxed potential energy surface scans performed at the B3LYP/6-31G(d) level identify the transition state (TS) and intermediate reaction species for $\text{Na}^+(\text{Asn})$ deamidation, structures that are further optimized at the B3LYP/6-311+G(d,p) level. Single-point energies of the key optimized structures are calculated at MP2(full), B3LYP, and B3P86 levels using a 6-311+G(2d,2p) basis set. This coordinated application of both experimental work and quantum chemical calculations allows for a complete characterization of the elementary steps of this reaction and identification of the rate-limiting elementary step of Asn deamidation. The latter is measured to require 1.61 ± 0.08 eV and involves formation of a cyclic succinic ring structure.

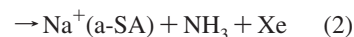
Introduction

The deamidation of asparagine residues is the most commonly observed form of post-translational protein modification. This spontaneous process plays both a productive and a destructive role in protein processing and has been linked to Alzheimer's disease,^{1,2} Parkinsons disease,³ HIV,⁴ and various forms of cancer.^{5,6} The generally accepted mechanism for asparagine deamidation involves the formation of an intramolecular succinic ring structure, Figure 1, which can further break down biologically into a number of altered products found in proteins including aspartate, isoaspartate, and cyclic succinimide residues.⁷

Mechanistic studies in the solution phase have established that formation of the succinic ring is the rate-limiting step in asparaginyl residue deamidation,⁸ and computational studies have characterized ring formation in a model peptide.⁹ Additionally, both mechanistic and kinetic characterizations of this

process have been determined as a function of medium,⁹ temperature,¹⁰ viscosity,^{11,12} pH,^{13,14} and protein sequence.³ However, these are mostly large-scale studies and are unable to experimentally investigate intrinsic molecular interactions with accuracy and precision. A description of the precise series of molecular rotations and translocations that must be undergone in this reaction can only be accomplished in an environment free of complications including those from solvent effects. Thus, measurement of gas-phase decomposition is potentially insightful and has the additional advantage of reflecting the intrinsic bond strengths and molecular transformation energies for asparagine deamidation. Further, this is an ideal venue for a detailed comparison of experimental and theoretical results including a complete characterization of the elementary steps undergone in this reaction.

We recently reported that the collisional activation of $\text{Na}^+(\text{Asn})$ in a guided ion beam tandem mass spectrometer at low collision energies yields both loss of the intact amino acid and loss of NH_3 , reactions 1 and 2.¹⁵



- (1) Shimizu, T.; Watanabe, A.; Ogawara, M.; Mori, H.; Shirasawa, T. *Arch. Biochem. Biophys.* **2000**, *381*, 225.
- (2) Shimizu, T.; Fukuda, H.; Murayama, S.; Izumiyama, N.; Shirasawa, T. *J. Neurosci. Res.* **2002**, *70*, 451.
- (3) Robinson, N. E.; Robinson, A. B. *J. Pept. Res.* **2004**, *63*, 437.
- (4) Aswad, D. W. *Deamidation and Isoaspartate Formation in Peptides and Proteins*; CRC Press, Inc: Boca Raton, FL, 1995.
- (5) Deverman, B. E.; Cook, B. L.; Manson, S. R.; Niederhoff, R. A.; Langer, E. M.; Rosova, I.; Kulans, L. A.; Fu, X.; Weinberg, J. S.; Heinecke, J. W.; Roth, K. A.; Weintraub, S. J. *Cell* **2002**, 111.
- (6) Weintraub, S. J.; Manson, S. R. *Mech. Ageing Dev.* **2004**, *125*, 255.
- (7) Clarke, S. *Ageing Res. Rev.* **2003**, *2*, 263.
- (8) Capasso, S.; Kirby, A. J.; Salvadori, S.; Sica, F.; Zagari, A. *J. Chem. Soc., Perkin Trans. 2* **1995**, 437.
- (9) Konuklar, F. A.; Aviyente, V.; Sen, T. Z.; Bahar, I. *J. Mol. Model.* **2001**, *7*, 147.

- (10) Patel, K.; Borchardt, R. T. *Pharm. Res.* **1990**, *7*, 703.
- (11) Tyler-Cross, R.; Schirch, V. *J. Biol. Chem.* **1991**, *266*, 22549.
- (12) Song, Y.; Schowen, R. L.; Borchardt, R. T.; Topp, E. M. *J. Pharm. Sci.* **2001**, *90*, 141.
- (13) Capasso, S.; Mazzarella, L.; Sica, F.; Zagari, A.; Salvadori, S. *J. Chem. Soc., Perkin Trans. 2* **1993**, 679.

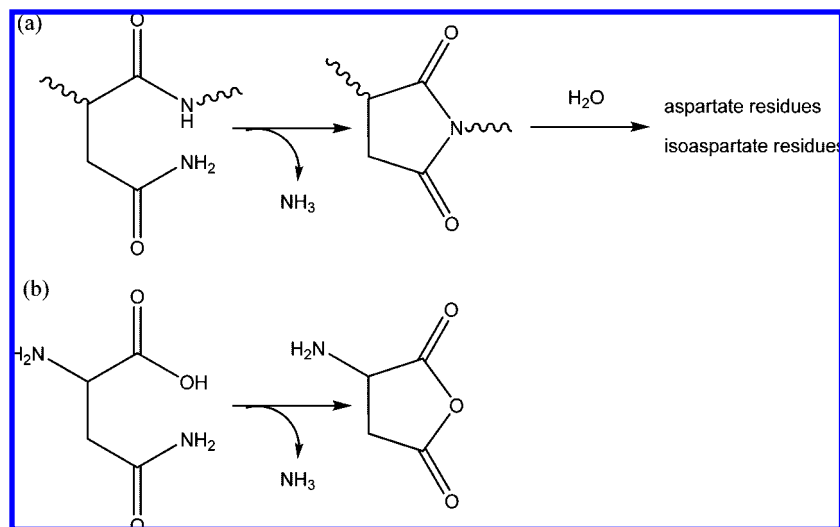


Figure 1. Reaction pathway for deamidation (a) in an asparaginyl residue within a peptide forming a succinimide residue that can further combine with H₂O and (b) in the monomeric amino acid asparagine forming 3-amino-succinic anhydride, a-SA.

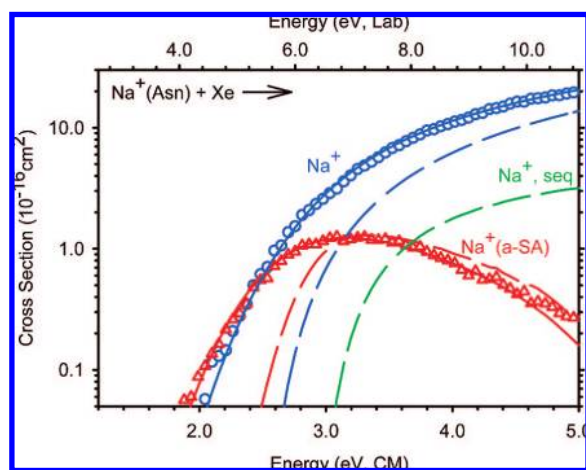


Figure 2. Experimental cross sections for collision-induced dissociation of Na⁺(Asn) with Xe as a function of kinetic energy in the center-of-mass frame (lower *x*-axis) and the laboratory frame (upper *x*-axis) for reactions 2 (red triangles) and 1 (blue circles). Solid lines show the best fit to the data using the models of eqs 4–6 convoluted over the neutral and ion kinetic and internal energy distributions. Dashed lines show the model cross sections for reactions 2, 1, and 3 (in order of increasing threshold energy) in the absence of experimental kinetic energy broadening for reactions with an internal energy of 0 K.

Figure 2 shows the collision-induced dissociation (CID) cross sections for reactant ions formed in an electrospray ionization (ESI) source. In addition to reactions 1 and 2, the cross section for the primary product of reaction 2 shows evidence for the sequential loss of the sodium cation, reaction 3, at higher energies. An additional CID study of this system utilizing reactant ions formed in a dc discharge/flow tube ion source produced primarily a bis-ligand complex of Na⁺(Asn-NH₃)(NH₃), from which the (Asn-NH₃) ligand was identified as 3-amino succinic anhydride (a-SA).¹⁶ As shown in Figure 1, this is the direct analogue of the deamidation product of asparagine observed in solution. The Na⁺ affinities of Asn and

a-SA were determined quantitatively in these studies as 209 ± 6 and 130 ± 5 kJ/mol, respectively.^{15,16} In the work presented here, we seek to fully characterize the deamidation of sodium-bound asparagine. We measure the first absolute experimental energetics for this reaction and use theoretical calculations at the B3LYP/6-311+G(d,p) level to provide structures, vibrational frequencies, and rotational constants needed for analysis of the deamidation reaction. Experimental threshold energies are compared to theoretical calculations performed at the B3LYP, B3P86, and MP2(full) levels using a 6-311+G(2d,2p) basis set in order to fully characterize the rate-limiting elementary step of asparagine deamidation. In addition, the theoretical calculations provide a detailed step-by-step pathway for this process.

Experimental and Computational Section

Thermochemical Analysis. The acquisition of the experimental data analyzed here, Figure 2, has been fully described in our previous publication.¹⁵ Because the system involves two competing reactions, processes 1 and 2, the CID reaction cross sections are modeled using eq 4,

$$\sigma_j(E) = (n\sigma_{0j}/E) \sum g_i \int_{E_{0j}-E_i}^E [k_j(E^*)/k_{\text{tot}}(E^*)] P_{D1} \times (E - \epsilon)^{n-1} d\epsilon \quad (4)$$

where σ_{0j} is an energy-independent scaling factor for channel j , n is an adjustable parameter that describes the efficiency of collisional energy transfer,¹⁷ E is the relative kinetic energy of the reactants, E_{0j} is the threshold for CID of the ground electronic and rovibrational state of the reactant ion at 0 K for channel j , ϵ is the energy transferred from translation during the collision, and E^* is the internal energy of the energized molecule (EM) after the collision, i.e., $E^* = \epsilon + E_i$. The term $k_j(E^*)$ is the unimolecular rate constant for dissociation of the energized molecule to channel j . P_{D1} is the probability for dissociation of the EM and is given by $1 - \exp[-k_{\text{tot}}(E^*)\tau]$, where τ is the experimental time for dissociation ($\sim 5 \times 10^{-4}$ s in the extended dual octopole configuration as measured by time-of-flight studies),¹⁷ and k_{tot} is given below. The summation in eq 4 is over the rovibrational states of the reactant ions, i , where E_i is the excitation energy of each state and g_i is the fractional population of those states ($\sum g_i = 1$). This equation accounts for the lifetime for dissociation of the EM, which can lead to a delayed onset for the reaction threshold, a kinetic

(14) Peters, B.; Trout, B. L. *Biochemistry* **2006**, *45*, 5384.

(15) Heaton, A. L.; Moision, R. M.; Armentrout, P. B. *J. Phys. Chem. A* **2008**, *112*, 3319.

(16) Heaton, A. L.; Ye, S. J.; Armentrout, P. B. *J. Phys. Chem. A* **2008**, *112*, 3328.

(17) Muntean, F.; Armentrout, P. B. *J. Chem. Phys.* **2001**, *115*, 1213.

shift, which becomes more noticeable as the size of the complex increases. In addition, eq 4 naturally includes competition among parallel reactions in a full statistical treatment.¹⁸ Previous studies have verified its efficacy in modeling reactions that compete through loose as well as loose vs tight transition states.^{17,19–24}

The rate constants $k_j(E^*)$ necessary for competitive modeling¹⁸ and $k_{\text{tot}}(E^*)$ are defined by Rice–Ramsperger–Kassel–Marcus (RRKM) theory as in eq 5,^{25,26}

$$k_{\text{tot}}(E^*) = \sum_j k_j(E^*) = \sum_j d_j N_j^\ddagger(E^* - E_{0,j}) / h \rho(E^*) \quad (5)$$

where d_j is the reaction degeneracy of channel j , $N_j^\ddagger(E^* - E_{0,j})$ is the sum of rovibrational states of the transition state (TS) for channel j at an energy $E^* - E_{0,j}$, and $\rho(E^*)$ is the density of states of the energized molecule (EM) at the available energy, E^* . Vibrational frequencies and rotational constants are taken from quantum chemical calculations, as detailed in the next section. The Beyer–Swinehart algorithm^{27–29} is used to evaluate the number and density of the rovibrational states, and the relative populations g_j are calculated for a Maxwell–Boltzmann distribution at 300 K. For reactions 1 and 3, the transitional frequencies are treated as rotors, a treatment that corresponds to a phase space limit (PSL), as described in detail elsewhere.^{18,30} The 2D external rotations are treated adiabatically, but with centrifugal effects included,²⁹ and calculated using a statistical distribution with an explicit summation over all the possible values of the rotational quantum number. For reaction 2, a tight transition state is required, and all molecular parameters are taken from theoretical results.

Because the cross section for reaction 2 is also influenced by the sequential dissociation process 3, modeling of the data over an extended energy range also requires including this latter reaction. The additional assumptions needed to describe such processes have been described previously.³¹ The difficulty in analyzing sequential thresholds lies in the fact that the initial dissociation process takes away an unknown distribution of energies in translational modes of the initial products, here $\text{Na}^+(\text{a-SA}) + \text{NH}_3$, as well as internal modes of the neutral product, NH_3 . This leaves an unknown distribution of internal energies in the ionic product to undergo further dissociation, $\text{Na}^+(\text{a-SA})$. The procedure used to handle this effect uses eq 4 to reproduce the cross section for the $\text{Na}^+(\text{a-SA})$ product of reaction 2, which excludes subsequent dissociation, $\sigma_{\text{aSA}}(E)$, combined with the probability for further dissociation, $P_{\text{D}2} = 1 - \exp[-k_2(E_2^*)\tau_2]$. Here k_2 , E_2^* , and τ_2 are the rate constant for the secondary dissociation, the energy available to the secondary EM, $\text{Na}^+(\text{a-SA})$, and the time available for the secondary dissociation, respectively. This partitions the total CID cross section into that for the nondissociating products, $\text{Na}^+(\text{a-SA})$, and that for the dissociation products, $\text{Na}^+ + \text{a-SA}$. Equation 4 then becomes eqs 6,

$$\sigma_j[E, \text{Na}^+(\text{a-SA})] = \sigma_{\text{aSA}}(E)(1 - P_{\text{D}2}) \quad (6a)$$

$$\sigma_j[E, \text{Na}^+] = \sigma_{\text{aSA}}(E)P_{\text{D}2} \quad (6b)$$

- (18) Rodgers, M. T.; Armentrout, P. B. *J. Chem. Phys.* **1998**, *109*, 1787.
 (19) Muntean, F.; Armentrout, P. B. *J. Phys. Chem. B* **2002**, *106*, 8117.
 (20) Muntean, F.; Heumann, L.; Armentrout, P. B. *J. Chem. Phys.* **2002**, *116*, 5593.
 (21) Muntean, F.; Armentrout, P. B. *J. Phys. Chem. A* **2003**, *107*, 7413.
 (22) Narancic, S.; Bach, A.; Chen, P. *J. Phys. Chem. A* **2007**, *111*, 7006.
 (23) Ruan, C.; Yang, Z.; Rodgers, M. T. *Phys. Chem. Chem. Phys.* **2007**, *9*, 5902–5918.
 (24) Jia, B.; Angel, L. A.; Ervin, K. M. *J. Phys. Chem. A* **2008**, *112*, 1773.
 (25) Gilbert, R. G.; Smith, S. C. *Theory of Unimolecular and Recombination Reactions*; Blackwell Scientific: London, 1990.
 (26) Robinson, P. J.; Holbrook, K. A. *Unimolecular Reactions*; Wiley Interscience: New York, 1972.
 (27) Beyer, T. S.; Swinehart, D. F. *Commun. ACM* **1973**, *16*, 379.
 (28) Stein, S. E.; Rabinovitch, B. S. *J. Chem. Phys.* **1973**, *58*, 2438.
 (29) Stein, S. E.; Rabinovitch, B. S. *Chem. Phys. Lett.* **1977**, *49*, 183.
 (30) Rodgers, M. T.; Ervin, K. M.; Armentrout, P. B. *J. Chem. Phys.* **1997**, *106*, 4499.

Table 1. Fitting Parameters of Eqs 4–6, Threshold Energies at 0 K, and Entropies of Activation at 1000 K for CID of $\text{Na}^+(\text{Asn})$ with Xe^a

reactant	products	σ_0	n	E_0 (eV)	ΔS^\ddagger_{1000} (J/K/mol)
$\text{Na}^+(\text{Asn})$	$\text{Na}^+ + \text{Asn}$	19.2 (3.2)	1.7 (0.1)	2.15 (0.07)	42.0 (2.1)
	$\text{Na}^+(\text{a-SA}) + \text{NH}_3$	4.0 (3.3)		1.61 (0.08)	-110.1 (7.0)
	$\text{Na}^+ + \text{a-SA} + \text{NH}_3^b$	75.8 (3.4)		2.83 (0.07)	-67.0 (5.5)

^aUncertainties in parentheses. ^bSequential sodium loss from $\text{Na}^+(\text{a-SA})$.

where the rate constants are again calculated using RRKM theory, eq 5, for the new EM, $\text{Na}^+(\text{a-SA})$. The energy available to this EM is defined statistically, accomplished by methods described in detail elsewhere.³¹ The combination of sequential and competitive modeling allows accurate reproduction of all experimentally observed reactions here.

Several effects that would otherwise obscure the interpretation of the data must also be accounted for during data analysis. The first effect involves energy broadening resulting from the thermal motion of the neutral collision gas and the kinetic energy distribution of the reactant ion, accounted for by explicitly convoluting the models of eqs 4 and 6 over both kinetic energy distributions.³² The second effect considers that our models only represent products formed as the result of a single collision event, accounted for by evaluating the cross sections for pressure effects and extrapolating to zero pressure of Xe (rigorously single collision conditions) when necessary.³³

After convolution with the kinetic energy distribution of the reactants, the model cross sections of eqs 4 and 6 are compared to the data. Because reactions 1 and 3 have the same ionic product, modeling of the Na^+ channel includes contributions from both pathways. A nonlinear least-squares analysis is used to provide optimized values for $\sigma_{0,j}$, n , and $E_{0,j}$. The uncertainty associated with $E_{0,j}$ is estimated from the range of threshold values determined from different data sets with variations in the parameter n , 10% variations in most vibrational frequencies and factors of 2 for the $\text{Na}^+(\text{L})$ modes, changes in τ by factors of 2, and the uncertainty of the absolute energy scale, 0.05 eV (laboratory).

Computational Details. Model structures, vibrational frequencies, and energetics for all reaction species, including all transition state and intermediate species, were calculated using Gaussian 03.³⁴ A series of relaxed potential energy surface (PES) scans at the B3LYP/6-31G(d) level were performed in order to identify the elementary steps of the asparagine deamidation reaction. Transition state and intermediate structures occurring along this PES were further optimized at the B3LYP/6-311+G(d,p) level, where each transition state was found to contain one imaginary frequency and each intermediate was vibrationally stable. Rotational constants were obtained from the optimized structures, and all vibrational frequencies were also calculated at this level. When used in internal energy determinations or for RRKM calculations, the vibrational frequencies were scaled by 0.99.³⁵ Zero-point vibrational energy (ZPE) corrections were additionally determined using the scaled vibrational frequencies. Ground state (GS) geometries for the reactant and product species of each reaction are taken from previous work,^{15,16} where a simulated annealing methodology was used to identify the GS conformations of these species,³⁶ and optimizations were

- (31) Armentrout, P. B. *J. Chem. Phys.* **2007**, *126*.
 (32) Ervin, K. M.; Armentrout, P. B. *J. Chem. Phys.* **1985**, *83*, 166.
 (33) Hales, D. A.; Lian, L.; Armentrout, P. B. *Int. J. Mass Spectrom. Ion Processes* **1990**, *102*, 269.
 (34) Frisch, M. J.; et al. *Gaussian 03*, revision B.02; Gaussian, Inc.: Pittsburgh, PA, 2003.
 (35) Montgomery, J. A., Jr.; Frisch, M. J.; Ochterski, J. W.; Petersson, G. A. *J. Chem. Phys.* **1999**, *110*, 2822.
 (36) Moision, R. M.; Armentrout, P. B. *J. Phys. Chem. A* **2006**, *110*, 3933.

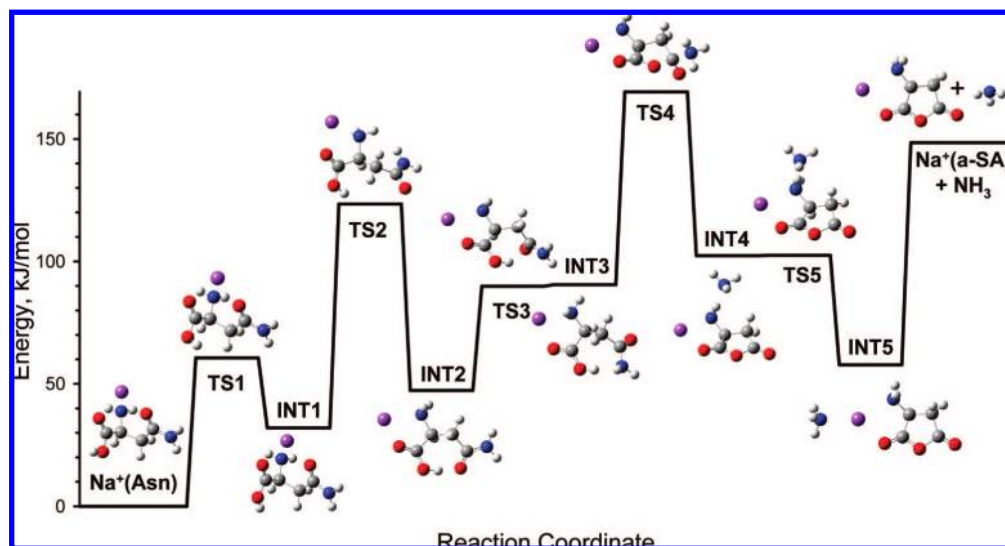


Figure 3. Potential energy surface for $\text{Na}^+(\text{Asn})$ deamidation. Geometry optimizations and single-point energies of each elementary step are determined at the B3LYP/6-311+G(d,p) level of theory.

performed at the B3LYP/6-311+G(d,p) level with single-point energies determined at the B3LYP, B3P86, and MP2(full) levels using the 6-311+G(2d,2p) basis set. For a direct comparison, key elementary structures in the present study are additionally determined at the B3LYP, B3P86, and MP2(full) levels using the 6-311+G(2d,2p) basis set and the B3LYP/6-311+G(d,p) geometries. Basis set superposition errors (BSSE) were estimated for all loose-TS dissociation channels, reactions 1 and 3, using the full counterpoise (cp) method.^{37,38} Clearly such BSSE corrections are not appropriate for the energy of a tight transition state, such as that for reaction 2.

Results

Threshold Analysis. The models of eqs 4 and 6 were used to analyze the thresholds for reactions 1–3. Figure 2 shows that the experimental cross sections are reproduced over a large range of energies (>3 eV) and magnitudes (greater than 2 orders of magnitude). The optimized fitting parameters are provided in Table 1. From our analysis, we also derive values of ΔS^\ddagger_{1000} , the entropy of activation at 1000 K, which give some idea of the looseness/tightness of the transition states, Table 1. This value for the sodium cation-loss channel, 42 J/K/mol, is in the range determined by Lifshitz³⁹ for simple bond cleavage dissociations of several ions. This is reasonable considering that the loose TS of this reaction is assumed to lie at the centrifugal barrier for the association of $\text{Na}^+ + \text{Asn}$. In contrast, ΔS^\ddagger_{1000} is highly negative for the deamidation reaction, -110 J/K/mol, a pathway that is modeled using a tight transition state. Further, the ΔS^\ddagger_{1000} value for sequential loss of Na^+ from a-SA, -67 J/K/mol, lies directly between these values. Again this makes sense, as the overall reaction pathway first passes through a tight TS in formation of the $\text{Na}^+(\text{a-SA})$ complex and then passes over a loose TS to yield free Na^+ and a-SA.

Note that the apparent difference in threshold energies for reactions 1 and 2 (on the order of 0.2 eV, Figure 2) is much smaller than that obtained from the modeling (0.54 ± 0.11 eV). This is a reflection of the much larger kinetic shift obtained for the tight transition state of reaction 2 compared to the loose

transition state for reaction 1. This difference is also reflected in the relative magnitudes of the two processes, such that reaction 2 has a smaller cross section at higher energies, even though it has a much lower threshold energy.

Theoretical Results for Asparagine Deamidation. The elementary steps for deamidation of sodiated asparagine were identified and calculated as described above. The potential energy surface of elementary steps leading to deamidation is provided in Figure 3. The relative energies and the molecular parameters of all reaction species are provided in Table 2. In the ground-state of the reactant $\text{Na}^+(\text{Asn})$ complex,¹⁵ Asn binds the sodium cation in a tridentate association, [N,CO,CO], with its two carbonyl oxygens and the nitrogen of the backbone amino group. This conformation is additionally stabilized by an $\text{OH}\cdots\text{O}=\text{C}$ hydrogen bond in the cis-COOH group. In the first elementary step of deamidation, this hydrogen bond is broken by rotation around the $\angle\text{HOCO}$ dihedral angle. The rotation causes the complex to pass TS1, characterized by a gauche-COOH orientation, and continuation of this rotation forms the stable INT1, characterized by a trans-COOH orientation and retention of the [N,CO,CO] association to Na^+ . In the second elementary step, a rotation of the $\angle\text{CCCC}$ dihedral angle breaks the tridentate binding to the sodium cation by passing TS2 and forming the stable INT2. In this intermediate, there is [N,CO] bidentate binding of the backbone to Na^+ , and the carbonyl oxygen of the side chain becomes hydrogen-bonded with the carboxylic acid group. In the third elementary step, rotation of the $\angle\text{CCCO}$ dihedral angle of the side chain breaks this hydrogen bond by passing TS3 but reforms a hydrogen bond with the amino nitrogen of the backbone to form INT3. Interestingly, TS3 and INT3 are nearly isoenergetic, such that zero-point energy correction results in INT3 being slightly higher in energy than TS3. The details of this elementary step are described in more detail below. In the fourth elementary step, the hydroxyl hydrogen transfers to the side-chain nitrogen while the hydroxyl oxygen of the backbone nears the carbon of the carboxamide functional group in a cyclization process, leading to the rate-limiting TS4. Free ammonia leaves and associates favorably with the amino nitrogen of the newly formed a-SA ligand to form INT4. In the fifth elementary reaction step, the ammonia molecule rearranges by passing TS5 to form the

(37) Boys, S. F.; Bernardi, R. *Mol. Phys.* **1970**, *19*, 553.

(38) van Duijneveldt, F. B.; van Duijneveldt de Rijdt, J. G. C. M.; van Lenthe, J. H. *Chem. Rev.* **1994**, *94*, 1873.

(39) Lifshitz, C. *Adv. Mass Spectrom.* **1989**, *11A*, 713–729.

Table 2. Bond Distances (Å), Bond Angles (°), and Relative Energies (kJ/mol) for Elementary Reaction Species of Deamidation of Sodium-Bound Asparagine^a

elementary reaction species	$r(\text{Na}^+-\text{O})^b$	$r(\text{Na}^+-\text{N})$	$r(\text{Na}^+-\text{X})$	$\angle(\text{N}-\text{Na}^+-\text{O}^b)$	$\angle(\text{N}-\text{Na}^+-\text{X})$	$\angle(\text{O}^b-\text{Na}^+-\text{X})$	energy, kJ/mol
$\text{Na}^+(\text{Asn})[\text{N},\text{CO},\text{CO}]\text{cis-COOH}$	2.318	2.479	2.230 ^c	69.8	79.6 ^c	88.3 ^c	0.0
TS1 $[\text{N},\text{CO},\text{CO}]\text{gauche-COOH}$	2.326	2.484	2.246 ^c	68.5	79.6 ^c	87.8 ^c	60.6
INT1 $[\text{N},\text{CO},\text{CO}]\text{trans-COOH}$	2.289	2.510	2.222 ^c	69.2	79.0 ^c	88.4 ^c	32.0
TS2 $[\text{N},\text{CO}]$	2.200	2.518		70.8			123.5
INT2 $[\text{N},\text{CO}]\text{COOH-O}$	2.178	2.488		69.9			47.3
TS3 $[\text{N},\text{CO}]$	2.206	2.470		70.6			89.9
INT3 $[\text{N},\text{CO}]\text{COOH-N}$	2.200	2.474		70.5			90.5
TS4 $[\text{N},\text{CO}]^d$	2.192	2.500		73.9			169.3
INT4 $[\text{N},\text{CO}](\text{NH}-\text{NH}_3)$	2.253	2.457	4.371 ^e	74.7	43.8 ^e	82.1 ^e	102.4
TS5 $[\text{N},\text{CO}]$	2.252	2.458	4.437 ^e	74.7	42.5 ^e	82.2 ^e	102.5
INT5 $[\text{N},\text{CO}](\text{Na}^+-\text{NH}_3)$	2.284	2.576	2.396 ^e	71.8	151.0 ^e	137.1 ^e	57.8
$\text{Na}^+(\text{a-SA})[\text{N},\text{CO}] + \text{NH}_3^f$	2.247	2.532		73.1			148.5

^a Structures calculated at B3LYP/6-311+G(d,p). ^b Carbonyl oxygen of amino acid backbone. ^c X = Carbonyl oxygen of amino acid side chain. ^d Rate-limiting transition state. ^e X = Nitrogen of free ammonia. ^f Dissociated products.

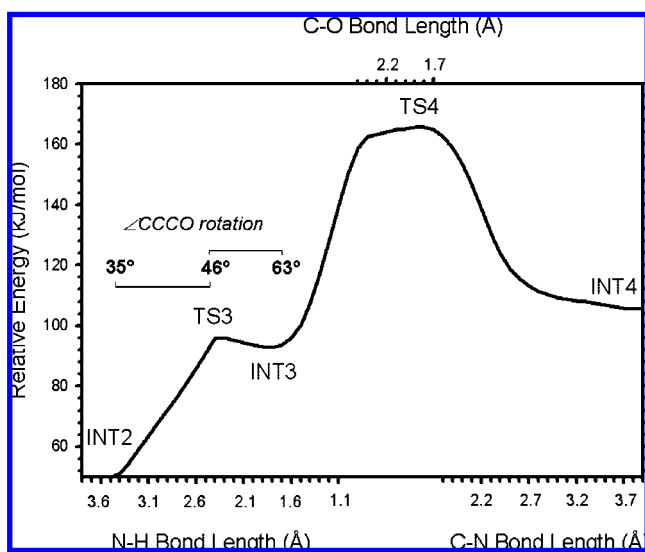


Figure 4. Relaxed potential energy surface scans for $\text{Na}^+(\text{Asn})$ deamidation involving the transformation from INT2 to INT4, performed at the B3LYP/6-31G(d) level of theory. All energies are relative to ground-state $\text{Na}^+(\text{Asn})$ calculated at this same level of theory.

ground-state bis-ligand complex, INT5, in which the ammonia binds directly to the sodium cation, as characterized in a previous study on the energetics of ligand binding in this complex.¹⁶ The last step of the deamidation reaction is the simple dissociation of the INT5 complex to form the $\text{Na}^+(\text{a-SA})$ and NH_3 products,¹⁶ which could also occur from INT4.

The transformation between INT3 and INT4 seems particularly complicated and hence was examined in more detail. A segment of the relaxed potential energy surface scan that involves this step is provided in Figure 4. This surface scans the energy of reaction as a function of bond length in three segments, N–H, C–O, and C–N, where in each segment the designated bond length is the only parameter fixed. Figure 4 begins with INT2 and proceeds by 0.1 Å stepwise decreases in the N–H bond length from 3.6 to 1.1 Å. In the first stage from INT2 to TS3, $r(\text{NH}) = 3.58\text{--}2.43$ Å, this motion is effectively coupled with rotation around the side-chain $\angle\text{CCCO}$ dihedral angle from 34.8° to 45.6° . TS3 corresponds to an energetic barrier that breaks the hydrogen bond between the backbone hydroxyl and side-chain carbonyl oxygen atoms. From TS3, the structure falls into the shallow energetic well of INT3, $r(\text{NH}) = 2.00$ Å and $\angle\text{CCCO} = 62.9^\circ$. This intermediate is nearly isoenergetic with TS3 at the B3LYP/6-311+G(d,p) level of

theory, lying 1.0 kJ/mol lower in energy than TS3 before ZPE corrections and 0.6 kJ/mol higher in energy than TS3 after ZPE corrections, Figure 3. Interestingly, if rotation around the $\angle\text{CCCO}$ dihedral angle in INT2 proceeds in the opposite direction, an intermediate analogous to INT3 cannot be achieved because the favorable hydrogen bonding interaction between the backbone amino group and side-chain oxygen cannot occur. Instead, this alternative surface moves directly from INT2 to a rate-limiting TS, which is calculated to be only slightly higher in energy than TS4, by 2–4 kJ/mol depending on the level of theory. Referring back to Figure 4, as the scan along the reaction coordinate proceeds beyond INT3 such that the N–H bond length decreases from 1.7 to 1.1 Å, there is a steep increase in energy that results from hydrogen transfer from the carboxylic acid OH to the amide nitrogen. At this point, the second segment of the surface scan proceeds by 0.1 Å stepwise decreases in the C–O bond length from 2.5 to 1.7 Å, resulting in closure of the five-membered ring. The maximum energy along the potential energy surface occurs in this segment, $r(\text{CO}) = 1.72$ Å, leading to the energetic barrier of the rate-limiting TS4. Subsequently, the third segment corresponds to 0.1 Å stepwise increases in the bond length of the free ammonia nitrogen and the carbon to which it was previously attached starting at $r(\text{C}-\text{N}) = 1.77$ Å. This causes detachment of the ammonia ligand from the newly formed a-SA succinic ring-complex to form INT4 at $r(\text{C}-\text{N}) = 4.79$ Å. An intrinsic reaction coordinate (IRC) calculation from TS4 verifies formation of the CN bond and cleavage of the ring when scanning toward INT3 and concurrent ring-closure and ammonia ligand-loss as the result of scanning toward INT4.

Discussion

Comparison of Experimental, Theoretical, and Literature Values. Experimental threshold energies for decomposition of $\text{Na}^+(\text{Asn})$ using TCID experiments with a guided ion beam mass spectrometer are compared to calculated quantum chemical reaction energies and available literature values in Table 3. Some previously determined values are available for the sodium cation affinity of asparagine from Kish et al.,⁴⁰ as well as from previous experiments in our laboratory,¹⁵ in which the competition with reaction 2 was ignored, Table 3. These values are in excellent agreement with the sodium cation affinity of Asn determined in the current study, falling within experimental uncertainties

(40) Kish, M. M.; Ohanessian, G.; Wesdemiotis, C. *Int. J. Mass Spectrom.* **2003**, *227*, 509.

Table 3. Experimental and Theoretical Reaction Energies (kJ/mol)

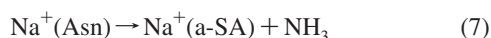
reactant	products	experiment ^a	B3LYP ^{b,c}	B3P86 ^{b,c}	MP2(full) ^b	MP2(full)(cp) ^{b,c}	literature
Na ⁺ (Asn)	Na ⁺ + Asn	207 (7)	220	210	216	203	209 (6) ^d , 204 (8) ^e
	Na ⁺ (a-SA) + NH ₃ , [TS4] ^f	155 (8)	168	163	165	165	
	Na ⁺ + a-SA + NH ₃	273 (7)	274	273	286	271	
		MAD ^g	9 (7)	4 (4)	11 (2)	5 (4)	

^a Present experimental values from Table 1. Uncertainties in parentheses. ^b Calculations performed at the stated level of theory using a 6-311+G(2d,2p) basis set with geometries calculated at the B3LYP/6-311+G(d,p) level. ^c Counterpoise corrected. ^d TCID results from Heaton et al.¹⁵ ^e Kinetic method results from Kish et al.⁴⁰ ^f Counterpoise not appropriate for tight TS. ^g Mean absolute deviation from experimental values.

in all cases. Additionally, the agreement between theory and experiment for each reaction observed here is extremely good. Theoretical calculations fall within the range of uncertainty of our experimentally determined thresholds in all cases. This includes the loose TS channels, Na⁺ loss from Na⁺(Asn), and dissociation of Na⁺(Asn) to form Na⁺ + a-SA + NH₃, as well as the tight TS reaction barrier for Na⁺(Asn) deamidation, which is inherently more difficult to characterize. This agreement supports the rate-limiting transition state found theoretically, TS4, as the correct barrier for this reaction, involving formation of the cyclic succinic ring structure.

A comprehensive evaluation of our theoretical numbers shows that values determined at the MP2(full) level excluding counterpoise corrections have a mean absolute deviation (MAD) from our experimentally determined values of 11 kJ/mol. By comparison, MP2(full) calculations including counterpoise have an MAD of 5 kJ/mol. Values calculated at the B3P86 level yield numbers that are in excellent agreement with experiment, with an MAD of 4 kJ/mol. Lastly, values calculated at the B3LYP level have an MAD of 9 kJ/mol. These variations are all comparable to the average experimental uncertainties of 7–8 kJ/mol.

As noted above, a previous study allowed the bond dissociation energy of Na⁺(a-SA) to be measured as 130 ± 5 kJ/mol.¹⁶ Given this energy and the threshold for reaction 3 measured here, 273 ± 7 kJ/mol, Table 3, we can calculate the energy of reaction 7 as 143 ± 9 kJ/mol.



Note that this is slightly below the threshold energy of reaction 2, in agreement with the potential energy landscape shown in Figure 3. Overall, even though the final products of reaction 2 are close in energy to TS4, TS4 is clearly the rate-limiting step in the deamidation process.

Conclusion

The kinetic energy dependence of the collision-induced dissociation of Na⁺(Asn) with Xe is examined in a guided ion

beam mass spectrometer. The threshold energy at 0 K for the Na⁺(Asn) deamidation, as well as the Na⁺ affinity of Asn and the energy for complete dissociation of Na⁺(Asn) to Na⁺ + a-SA + NH₃, is determined after consideration of the effects of reactant internal energy, multiple collisions with Xe, and lifetime effects.³⁰ The experimental results for the Na⁺(Asn) reactions, modeled with consideration of complex competitive and sequential processes, are in excellent agreement with quantum chemical calculations using the B3P86/6-311+(2d,2p)//B3LYP/6-311+G(d,p) level of theory, as well as with available literature values. The threshold reported here for the deamidation of Na⁺(Asn) constitutes the first experimental gas-phase measurement of this reaction. The theoretical calculations supported by experimental results permit a systematic evaluation of the precise series of molecular rotations and translocations that must be undergone in this reaction, including identification of the rate-limiting transition state, which dictates the threshold energy of reaction. In agreement with solution phase studies, the formation of a succinic ring structure is clearly the rate-limiting step in the deamidation of asparagine. The spontaneity of the biological reaction indicates that the 155 ± 8 kJ/mol barrier measured here must decrease in more complicated systems. Factors influencing this barrier include (a) in a peptide, the rate-limiting nucleophilic addition–elimination step involves a peptidic nitrogen rather than the acidic OH group considered here; (b) steric and energetic effects of the C-terminal residue side chains; (c) higher-order structural considerations; and (d) effects of hydration. Studies of these effects are underway.

Acknowledgment. This work is supported by the National Science Foundation, Grant CHE-0748790. A grant of computer time from the Center for High Performance Computing at the University of Utah is gratefully acknowledged.

Supporting Information Available: Full author list for ref 34. This material is available free of charge via the Internet at <http://pubs.acs.org>.

JA801726G